CHAPTER 9

Electronic supporting information

Contents

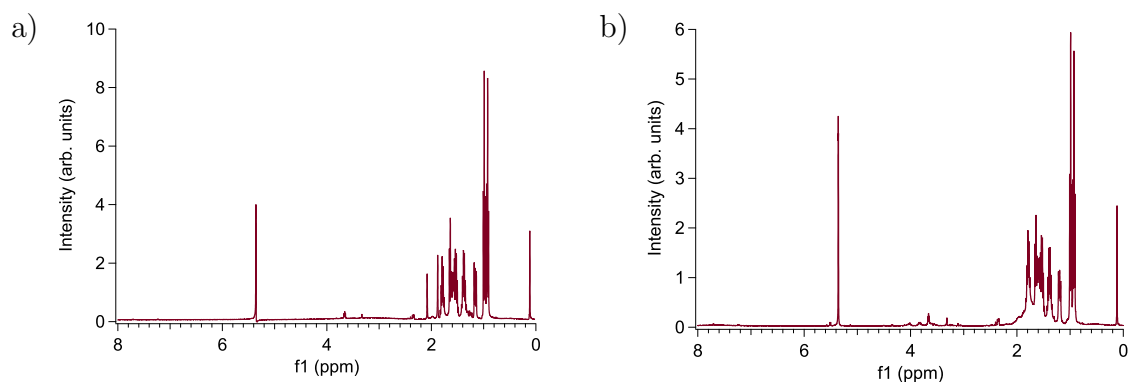## 9.2   Extreme ultraviolet patterning of tin-oxo cages

a)

b)

Figure 9.1: 400 MHz NMR spectra of the tin-oxo cage compounds (a) TinA (acetate counterions) and (b) TinM (malonate counterions).

9.3 DUV exposure of a tin-oxo cage in solution
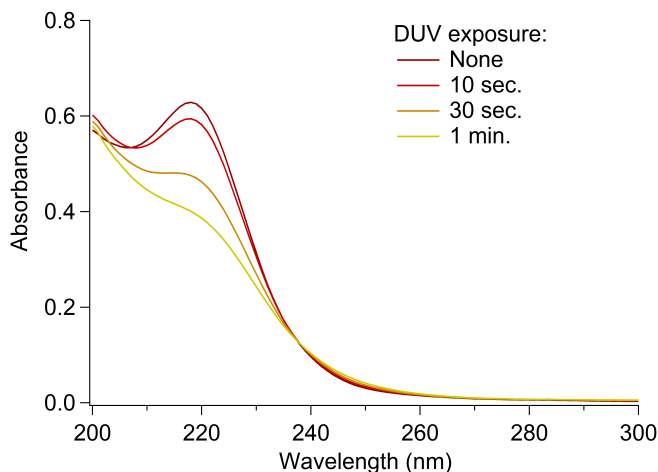
9.3.1 UV-visible spectroscopy

Figure 9.2: UV/VIS absorption spectra of TinOH in MeOH at different DUV exposure times (10 Hz, ∼1 mJ/pulse). Initial concentration is 4.5 µM.

9.3.2 NMR spectroscopy

^{119}Sn NMR

In Fig. 9.3 and 9.4 the ^{119}Sn NMR spectra of unexposed TinOTs (tosylate counterions) and TinOH (hydroxide counterions) in CDCl$_3$ are shown. In both spectra, two main peaks are present, which correspond to five-coordinated tin atoms (Sn$_5$) in the hexameric cycle and six-coordinated tin atoms (Sn$_6$) in the trimeric units. For TinOTs, these arise at -283.1 ppm and -462.3 ppm, respectively. Around these two
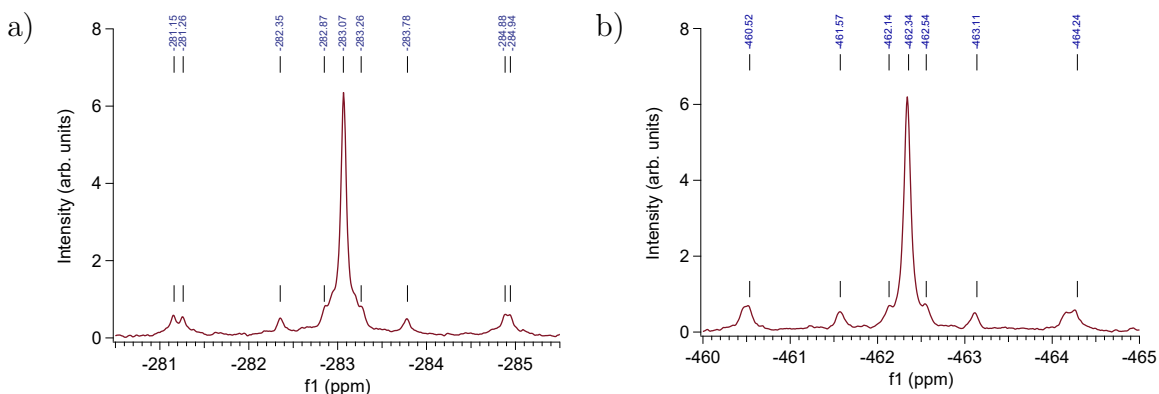

Figure 9.3: Proton-decoupled ^{119}Sn NMR of TinOTs recorded in CDCl$_3$. (a) 5-coordinated tin atoms, (b) 6-coordinated tin atoms.
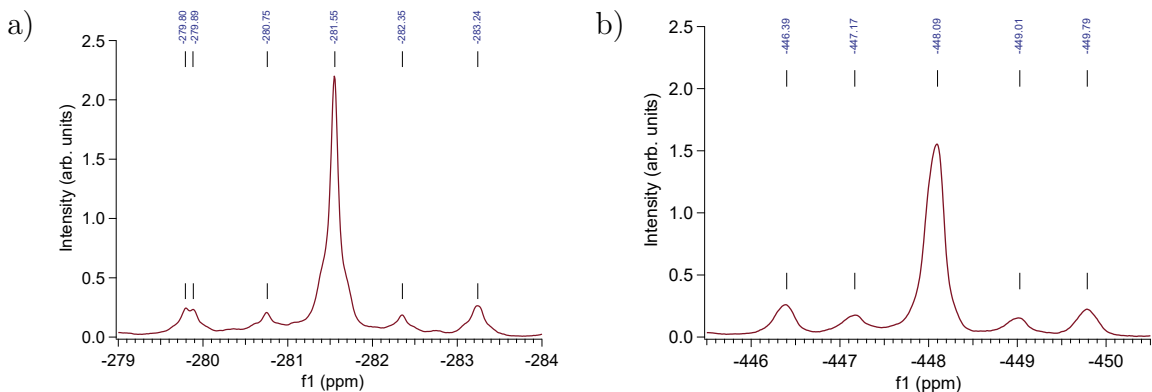
Figure 9.4: Proton-decoupled ^{119}Sn NMR of TinOH recorded in CDCl$_3$. (a) 5-coordinated tin atoms, (b) 6-coordinated tin atoms.

peaks, satellites can be seen that describe the connection between the different tin atoms through double or single oxo and oxo-hydroxo bridges (see Fig. 9.3 and Table 9.1).

Table 9.1: Satellites for $[(BuSn)_{12}(\mu_3\text{-}O)_{14}(\mu_2\text{-}OH)_6]$ $(O_3SC_6H_4CH_3)_2$ (TinOTs). Assignment based on Ref.[1].

δ Sn (ppm)	Isotope and environment	Path
Five-coordinated tin		
-281.15/-284.94	$^{119}Sn_6 - {}^{119/117}Sn_5$	Single oxo bridge
-282.35/-283.78	$^{119}Sn_5 - {}^{117}Sn_5$	Double oxo bridge
-282.87/-283.07/-283.26	$^{119}Sn_6 - {}^{119/117}Sn_5$	Double oxo bridge
Six-coordinated tin		
-460.52/-464.24	$^{119}Sn_6 - {}^{119/117}Sn_5$	Single oxo bridge
-461.57/-463.11	$^{119}Sn_6 - {}^{117}Sn_6$	Dbl. oxo-hydroxo bridge
-462.14/-462.34/-462.54	$^{119}Sn_6 - {}^{119/117}Sn_5$	Dbl. oxo bridge

Between TinOH and TinOTs, a large shift of the peak corresponding to the six-coordinated tin atom can be observed. In TinOTs, this peak is located at -462.3 ppm while for TinOH it is observed at -448.1 ppm. This is a shift of approximately 14 ppm, while the shift corresponding to the five-coordinated tin atoms is only 1.5 ppm. The positive charge of the tin-oxo cage is mostly located on the trimeric caps with the six-coordinated tin atoms. The environment of these tin atoms changes more strongly upon anion exchange, which results in this strong shift to higher ppm values.[2]
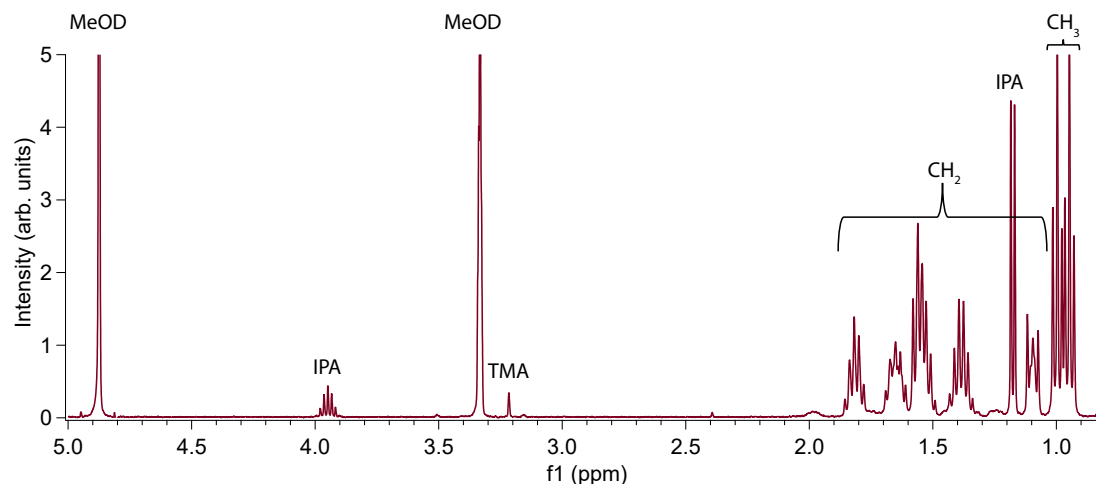
Figure 9.5: 400 MHz ^{1}H NMR spectrum of TinOH in MeOH-d_4.

^{1}H NMR

In Fig. 9.5, the NMR spectrum of TinOH in MeOH-d_4 is shown. The signals of CD_3OH and $CHCD_2OD$ are seen at 4.85 ppm and 3.31 ppm. iPrOH signals (3.95 ppm and 1.18 ppm) are present in the TinOH sample, because iPrOH is used in the crystallization step for the synthesis of TinOH. It has also been observed in the X-ray crystal structure of TinOH, and it was reported to be important for the stability of the crystals.[1,2] At around 3.2 ppm, a small peak is observed that corresponds to the tetramethylammonium cation chemical shift.[3] This ion is a residue from the synthesis of TinOH, which involves reacting TinOTs (tin-oxo cage with tosylate anions) with aqueous tetramethylammonium hydroxide.[2]

The assignment of the broad singlet at 1.96 ppm is unclear. The signal could be assigned to OH (either from the OH^- counter ions or the μ_2–bridged OH, both from the TinOH molecule), but the peak does not exhibit any solvent or temperature-dependent shifts characteristic of OH signals. The peak was also observed in previous studies.[1] All other peaks in the 1.79–0.92 ppm range (except for one iPrOH peak) correspond to TinOH. With 2D-TOCSY identical assignments to the literature could be made. Stability tests showed that the ^{1}H NMR spectrum did not change over relatively short time scales (4 hours). Hence, changes in the NMR spectrum upon DUV exposure can be related to the photochemistry of TinOH.

Signals of CH_2 protons in alkyl chains often look like simple symmetric multiplets, with $n+1$ lines for n equal ^3J couplings. The H atoms in a CH_2 group, however, are magnetically inequivalent, and in some cases this leads to very complicated splitting patterns. In the case of the n-butyltin oxo cages, only the CH_2 group next to the 6-coordinated Sn shows a complex pattern; all others show simple multiplets following the $n+1$ rule (see Table 9.2).

In Table 9.2 the integral values of the peaks are shown as well, with the integral of Sn_5-CH_2-**CH_2**-CH_2-CH_3 (1.82 ppm) used as a reference (set at 1.00). The peaks at 1.82, 1.65, 1.38 and 1.10 have the same number of corresponding protons, but their

Table 9.2: Assignments of ^{1}H NMR spectrum in Fig. 9.5. Integrals are calculated using the peak at 1.82 ppm as a reference.

δ (ppm)	Integral	Multiplicity	Assignment
1.99	0.10	Broad band	Unclear
1.82	1.00	Quintet	Sn_5-CH_2-**CH_2**-CH_2-CH_3
1.65	1.17	Quintet	Sn_6-CH_2-**CH_2**-CH_2-CH_3
1.59 – 1.48	2.22	Triplet/Sextet[a]	Sn_5-**CH_2**-CH_2-CH_2-CH_3 Sn_5-CH_2-CH_2-**CH_2**-CH_3
1.38	1.27	Sextet	Sn_6-CH_2-CH_2-**CH_2**-CH_3
1.19	1.11	Doublet	iPrOH
1.10	0.95	Multiplet[b]	Sn_6-**CH_2**-CH_2-CH_2-CH_3
1.00	1.75	Triplet	Sn_5-CH_2-CH_2-CH_2-**CH_3**
0.95	1.77	Triplet	Sn_6-CH_2-CH_2-CH_2-**CH_3**

[a]Because of overlapping signals, the multiplicity is not clear. The expected multiplicity from the structure is given. [b]Not a perfect triplet, as a result of an AA' system.

integrals are not completely identical. The (lack of) reliability of integral values can be related to the relaxation time T_1 between pulses.[4] Using the integral of the iPrOH peak, it is possible to calculate the amount of iPrOH present in TinOH powder. Approximately 1.3 iPrOH molecules are present in the TinOH sample, which is lower than the value of 4 reported by Banse and coworkers.[1] Using this information, the real amount of TinOH in TinOH powder can also be calculated.

Quantitative NMR

We can assume that the solubility in MeOH-d_4 is similar as in MeOH. The maximum amount of butane (or 1-butene) that can dissolve in methanol can be calculated using Eq. 9.1:

$$\frac{n_{\text{Bu}}}{n_{\text{Bu}} + n_{\text{MeOD}}} = x_{\text{Bu}} \tag{9.1}$$

In Eq. 9.1, n_{Bu} is the amount of generated butane (in mol), n_{MeOD} is the amount of MeOH-d_4, and $x_{\text{Bu}}(\approx 0.04)$ is the solubility of butane (in mol fraction).

After rewriting we obtain:

$$n_{\text{Bu}} = \frac{x_{\text{Bu}} \cdot n_{\text{MeOD}}}{1 - x_{\text{Bu}}} \tag{9.2}$$

The amount of methanol in the quartz NMR tube is around 0.6 mL (15 mmol). The maximum soluble amount of butane, as calculated by Eq. 9.2, is therefore around 0.6 mmol. In each experiment, approximately 21 mg (8.5 µmol) of TinOH is dissolved (or even less if some small amount of iPrOH in the powder is assumed). Therefore, the amount of butyl groups is around 0.1 µmol. If all these butyl groups were converted to butane, 0.1 µmol of butane would be generated. This is well below the solubility threshold of butane in our experiment (0.6 mmol, as calculated by Eq. 9.2). Therefore, we can assume that all butane and 1-butene remains in solution. Some butane or 1-butene could still evaporate as a result of the equilibrium with the atmosphere, but this is expected to be negligible.

iPrOH calculation

The absolute amount of iPrOH (n_{iPrOH}) should be known in order to calculate the amount of dissolved TinOH n_{TinOH}. This can be done by using integrals of iPrOH and tin-oxo cage signals (see Eq. 9.3). The TinOH CH_3 signals are reasonably isolated from other peaks and are therefore suitable for this calculation.

$$n_{\text{iPrOH}} \cdot \text{MW}_{\text{iPrOH}} + n_{\text{TinOH}} \cdot \text{MW}_{\text{TinOH}} = m_{\text{total}}$$
$$\frac{n_{\text{iPrOH}}}{n_{\text{TinOH}}} = \frac{36 \cdot I_{3.95}}{I_{1.03-0.92}} \tag{9.3}$$

In Eq. 9.3, m_{total} is the total mass dissolved in MeOH and I_δ is the integral value for the corresponding ppm value. The factor 36 appears because the iPrOH signal at 3.95 ppm corresponds to only one proton while the tin-oxo cage signal corresponds to 36 protons ($12 \times CH_3$). In the experiment, 21 mg of powder was dissolved, corresponding to 8.2 µmol (20 mg) of TinOH and 11 µmol (0.65 mg) of iPrOH (iPrOH:TinOH $\approx$ 1.6), as calculated by Eq. 9.3. Note that in the reported crystal structure, each TinOH is bound to 4 iPrOH molecules. It was already noted by Banse et al.[1] that crystals of TinOH · 4 iPrOH gradually lose iPrOH to form an amorphous powder.
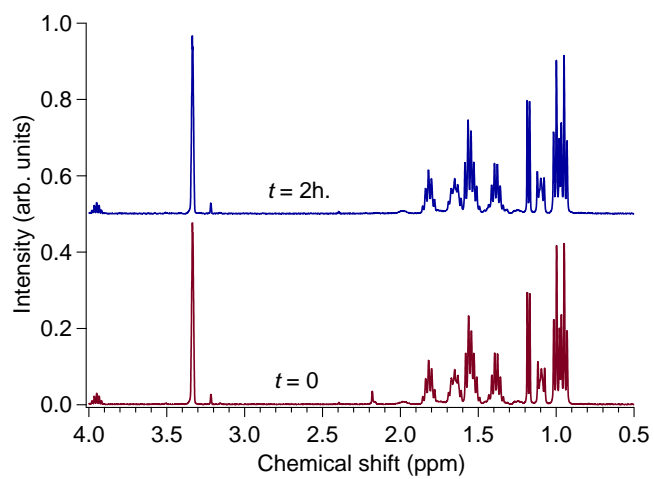
Figure 9.6: Stability test of TinOH in MeOH-d_4, at $t = 0$ (bottom) and $t = 2$h. (top).
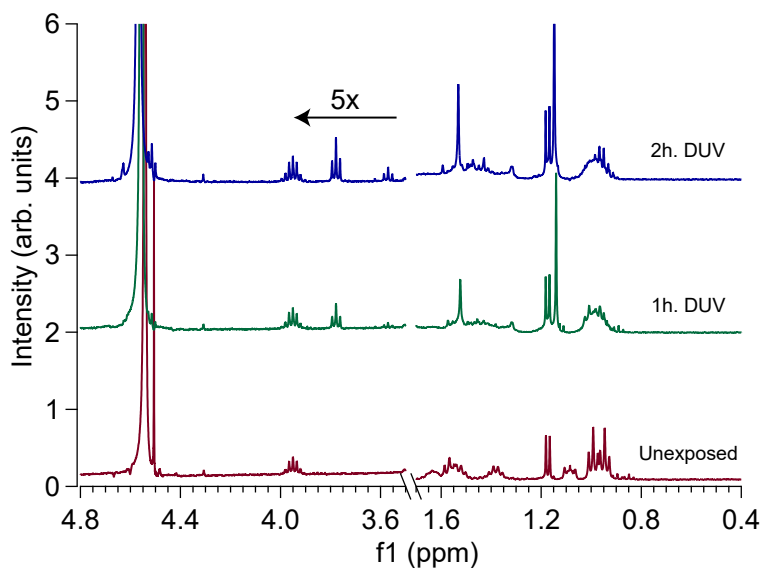

Figure 9.7: Full ^{1}H-NMR spectrum of TEMPO-adduct, appearing upon DUV exposure of a solution containing TEMPO and TinOH.

Table 9.3: Table showing all couplings in the 2D TOCSY spectrum of non-exposed TinOH in MeOH-d_4 (Fig. 3.8 in the main text).

Assignment (ppm)	^{1}H-^{1}H coupling with (ppm)
Sn$_5$-CH$_2$-**CH$_2$**-CH$_2$-CH$_3$ (1.79)	Sn$_5$-**CH$_2$**-CH$_2$-CH$_2$-CH$_3$ (1.56–1.48)[a] Sn$_5$-CH$_2$-CH$_2$-**CH$_2$**-CH$_3$ (1.56–1.48)[a] Sn$_5$-CH$_2$-CH$_2$-CH$_2$-**CH$_3$** (0.97)
Sn$_6$-CH$_2$-**CH$_2$**-CH$_2$-CH$_3$ (1.63)	Sn$_6$-CH$_2$-CH$_2$-**CH$_2$**-CH$_3$ (1.36) Sn$_6$-**CH$_2$**-CH$_2$-CH$_2$-CH$_3$ (1.07) Sn$_6$-CH$_2$-CH$_2$-CH$_2$-**CH$_3$** (0.92)
Sn$_5$-**CH$_2$**-CH$_2$-CH$_2$-CH$_3$ (1.56–1.48)/ Sn$_5$-CH$_2$-CH$_2$-**CH$_2$**-CH$_3$ (1.56–1.48)	Sn$_5$-CH$_2$-**CH$_2$**-CH$_2$-CH$_3$ (1.79) Sn$_5$-**CH$_2$**-CH$_2$-CH$_2$-CH$_3$ (1.56–1.48)/ Sn$_5$-CH$_2$-CH$_2$-**CH$_2$**-CH$_3$ (1.56–1.48) Sn$_5$-CH$_2$-CH$_2$-CH$_2$-**CH$_3$** (0.97)
Sn$_6$-CH$_2$-CH$_2$-**CH$_2$**-CH$_3$ (1.36)	Sn$_6$-CH$_2$-**CH$_2$**-CH$_2$-CH$_3$ (1.63) Sn$_6$-**CH$_2$**-CH$_2$-CH$_2$-CH$_3$ (1.07) Sn$_6$-CH$_2$-CH$_2$-CH$_2$-**CH$_3$** (0.92)
Sn$_6$-**CH$_2$**-CH$_2$-CH$_2$-CH$_3$ (1.07)	Sn$_6$-CH$_2$-**CH$_2$**-CH$_2$-CH$_3$ (1.63) Sn$_6$-CH$_2$-CH$_2$-**CH$_2$**-CH$_3$ (1.36) Sn$_6$-CH$_2$-CH$_2$-CH$_2$-**CH$_3$** (0.92)
Sn$_5$-CH$_2$-CH$_2$-CH$_2$-**CH$_3$** (0.97)	Sn$_5$-CH$_2$-**CH$_2$**-CH$_2$-CH$_3$ (1.79) Sn$_5$-**CH$_2$**-CH$_2$-CH$_2$-CH$_3$ (1.56–1.48)/ Sn$_5$-CH$_2$-CH$_2$-**CH$_2$**-CH$_3$ (1.56–1.48)
Sn$_6$-CH$_2$-CH$_2$-CH$_2$-**CH$_3$** (0.92)	Sn$_6$-CH$_2$-**CH$_2$**-CH$_2$-CH$_3$ (1.63) Sn$_6$-**CH$_2$**-CH$_2$-CH$_2$-CH$_3$ (1.36) Sn$_6$-CH$_2$-CH$_2$-**CH$_2$**-CH$_3$ (1.07)

[a]Multiplets overlap.

Table 9.4: Table showing all couplings in the 2D TOCSY spectrum of 2.5h. DUV-exposed TinOH in MeOH-d_4 (Figs. 3.18 and 3.19 in the main text).

Assignment (ppm)	^{1}H-^{1}H coupling with (ppm)
Butyraldehyde (9.7)	-
Acetal (4.48)	1.55
	1.40
	0.93
n-butanol (3.55)	1.61[a]
	1.52
	1.40
	0.94
Butyraldehyde (2.41)	0.90–0.95[a]
1-butene (2.05)	0.98
Sn_5-CH$_2$-**CH$_2$**-CH$_2$-CH$_3$ (1.81)	Sn_5-**CH$_2$**-CH$_2$-CH$_2$-CH$_3$ (1.67)
	Sn_5-CH$_2$-CH$_2$-**CH$_2$**-CH$_3$ (1.53)
	Sn_5-CH$_2$-CH$_2$-CH$_2$-**CH$_3$** (0.99)
Sn_5-**CH$_2$**-CH$_2$-CH$_2$-CH$_3$ (1.67)	Sn_5-CH$_2$-**CH$_2$**-CH$_2$-CH$_3$ (1.81)
	Sn_5-CH$_2$-CH$_2$-**CH$_2$**-CH$_3$ (1.53)
	Sn_5-CH$_2$-CH$_2$-CH$_2$-**CH$_3$** (0.99)
Sn_6-CH$_2$-**CH$_2$**-CH$_2$-CH$_3$ (1.63)	Sn_6-CH$_2$-CH$_2$-**CH$_2$**-CH$_3$ (1.40)
	Sn_6-**CH$_2$**-CH$_2$-CH$_2$-CH$_3$ (1.18)
	Sn_6-CH$_2$-CH$_2$-CH$_2$-**CH$_3$** (0.94)
Sn_5-CH$_2$-CH$_2$-**CH$_2$**-CH$_3$ (1.53)	Sn_5-CH$_2$-**CH$_2$**-CH$_2$-CH$_3$ (1.81)
	Sn_5-**CH$_2$**-CH$_2$-CH$_2$-CH$_3$ (1.67)
	Sn_5-CH$_2$-CH$_2$-CH$_2$-**CH$_3$** (0.99)
Sn_6-CH$_2$-CH$_2$-**CH$_2$**-CH$_3$ (1.40)	Sn_6-CH$_2$-**CH$_2$**-CH$_2$-CH$_3$ (1.63)
	Sn_6-**CH$_2$**-CH$_2$-CH$_2$-CH$_3$ (1.18)
	Sn_6-CH$_2$-CH$_2$-CH$_2$-**CH$_3$** (0.94)
n-butane/n-octane (1.29)	0.89
Sn_6-**CH$_2$**-CH$_2$-CH$_2$-CH$_3$ (1.18)	Sn_6-CH$_2$-**CH$_2$**-CH$_2$-CH$_3$ (1.63)
	Sn_6-CH$_2$-CH$_2$-**CH$_2$**-CH$_3$ (1.40)
	Sn_6-CH$_2$-CH$_2$-CH$_2$-**CH$_3$** (0.94)
Sn_5-CH$_2$-CH$_2$-CH$_2$-**CH$_3$** (0.99)	Sn_5-CH$_2$-**CH$_2$**-CH$_2$-CH$_3$ (1.81)
	Sn_5-**CH$_2$**-CH$_2$-CH$_2$-CH$_3$ (1.67)
	Sn_5-CH$_2$-CH$_2$-**CH$_2$**-CH$_3$ (1.53)
Sn_6-CH$_2$-CH$_2$-CH$_2$-**CH$_3$** (0.94)	Sn_6-CH$_2$-**CH$_2$**-CH$_2$-CH$_3$ (1.63)
	Sn_6-CH$_2$-CH$_2$-**CH$_2$**-CH$_3$ (1.40)
	Sn_6-**CH$_2$**-CH$_2$-CH$_2$-CH$_3$ (1.18)
n-butane/n-octane (0.89)	1.29

[a]Coupling not clearly resolved.

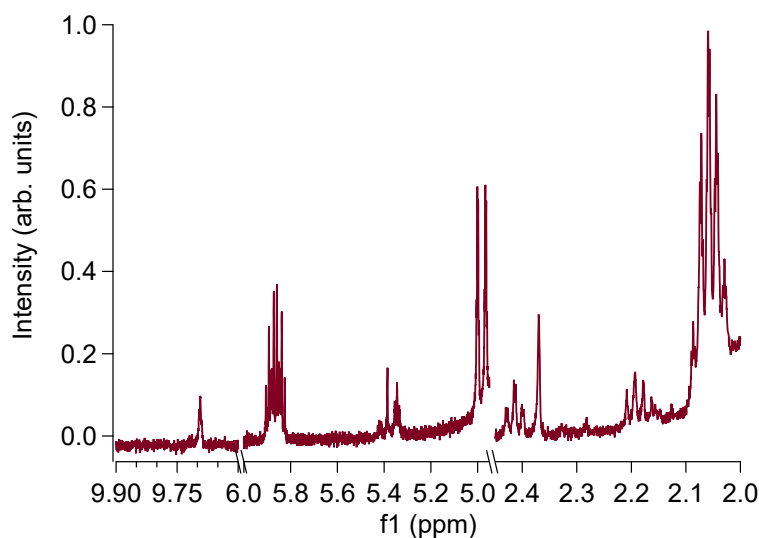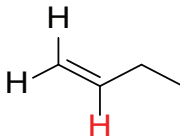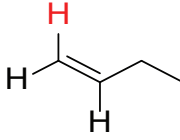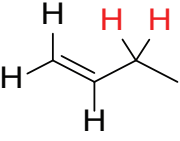Figure 9.8: ^{1}H NMR spectrum (zoomed in on selected products) of TinOH in MeOH-d_4, exposed to 150 min. DUV radiation, in a quartz NMR tube.

Table 9.5: Assignments of signals from Fig. 3.15 to 1-butene.[5]

δ (ppm)	Integral	Multiplicity	J(Hz)	Assignment
5.86	1.00	Doublet of doublet of triplet	$^3J_{\text{H-H,trans}} = 16.7$ $^3J_{\text{H-H,cis}} = 10.2$ $^3J_{\text{H-CH}_2} = 1.9$	
4.98	2.34	Doublet of quartet	$^3J_{\text{H-H,trans}} = 16.7$ $^2J_{\text{H-H,gem}} = 1.9$ $^4J_{\text{H-CH}_2} = 1.9$	
2.06	3.95	Doublet of doublet of doublet of quartet	$^3J_{\text{CH}_2\text{-CH}_3} = 9.2$ $^3J_{\text{CH}_2\text{-H}} = 6.2$ $^4J_{\text{CH}_2\text{-H}} = 1.9$ $^4J_{\text{CH}_2\text{-H}} = 1.6$	
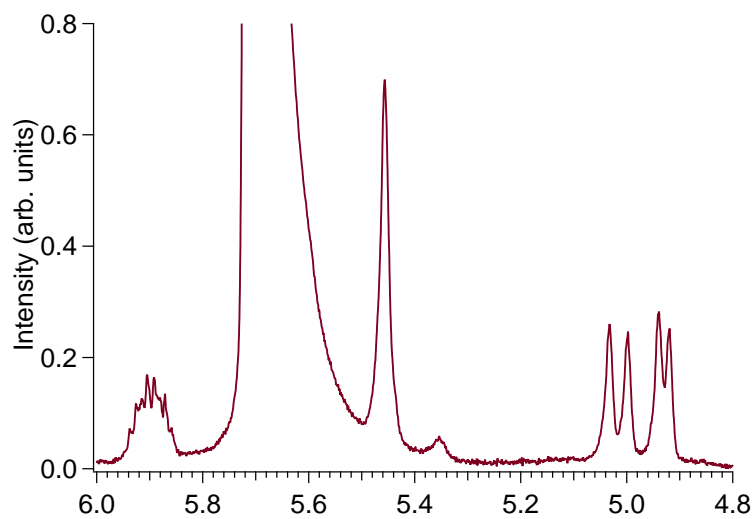
Figure 9.9: 2.5h. DUV exposed TinOH in MeOH-d_4 at –80 °C, zoomed in on the terminal CH_2 signal of 1-butene (4.98 ppm), now visible as a result of cooling.

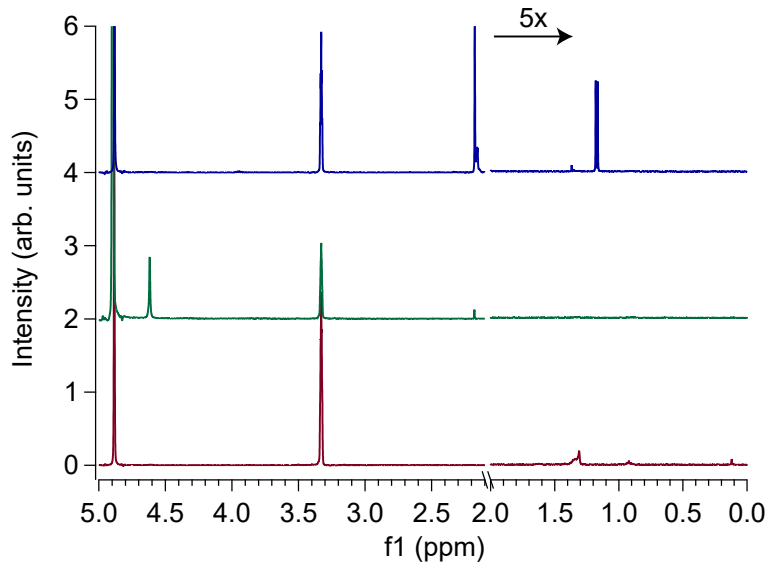Figure 9.10: 400 MHz ^{1}H NMR spectra of MeOD (red, bottom), distilled MeOD (green, middle), and distilled MeOD+TinOH (blue, top).
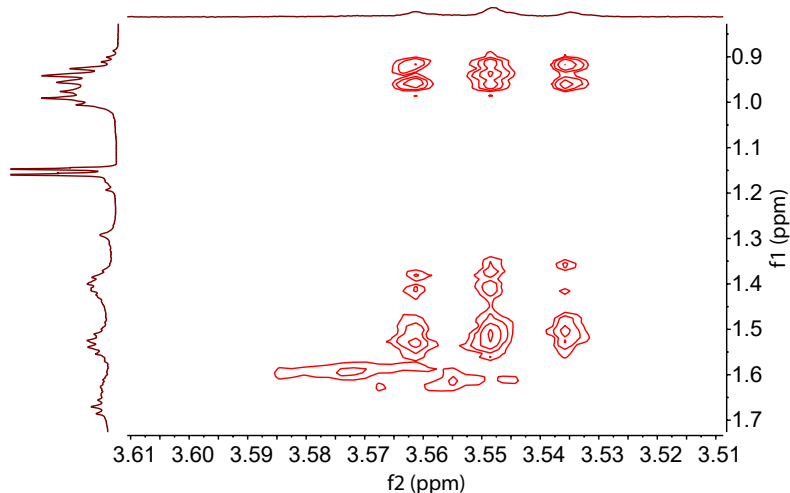
Figure 9.11: Closer look at the 2D TOCSY spectrum (Fig. 3.18) (peak at 3.55 ppm).

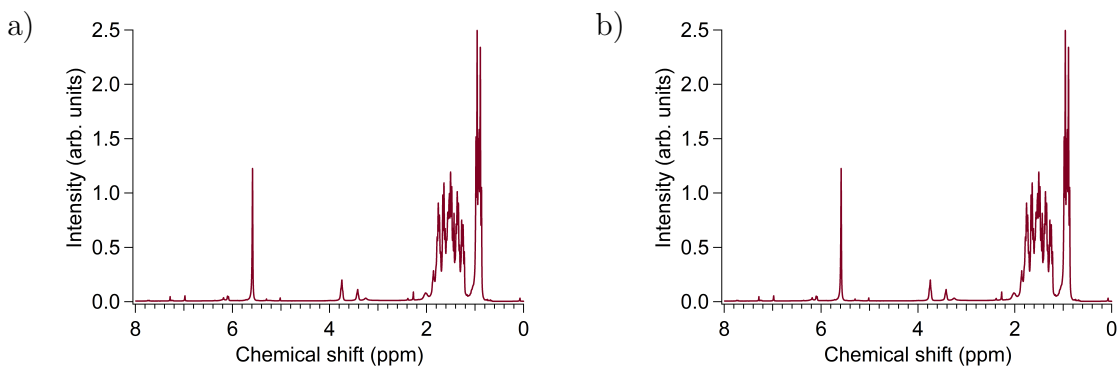## 9.4 UV and VUV-induced fragmentation of a tin-oxo cage compound

9.4.1 TinOTf characterization

Figure 9.12: (a) ^{1}H NMR spectrum and (b) ^{19}F NMR spectrum of TinOTf in CD_2Cl_2. The ^{1}H NMR shows the signals corresponding to butyl groups of the tin-oxo cage (see Chapter 3) and a signal for CD_2Cl_2 (5.4 ppm). The ^{19}F spectrum shows that only one type of fluorine atoms is present in the material.
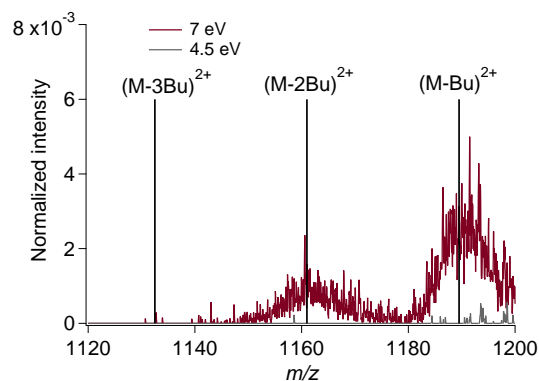
Figure 9.13: Photofragmentation spectrum of the tin-oxo cage dication at 7 eV (red) and 4.5 eV (gray). It can be seen that the 4.5 eV spectrum does not show a clear $(M–Bu)^{2+}$ or $(M–2Bu)^{2+}$ peak: the non-zero area between m/z 1175 and 1203 is due to spectral noise.
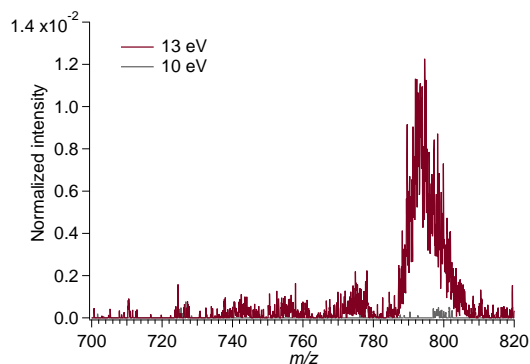

Figure 9.14: Photofragmentation spectrum of the tin-oxo cage dication at 13.0 eV (red) and 10.0 eV (gray). It can be seen that the 10.0 eV spectrum does not show a clear $(M–Bu)^{3+}$ peak: the non-zero area between m/z 786 and 800 is due to spectral noise.

9.5 Soft X-ray fragmentation of tin-oxo cage ions

9.5.1 Experimental methods (supplemental)

The dodecameric "tin-oxo cage" TinOH was synthesized using previously described methods (see Chapter 2). A solution of 0.1 mg/mL TinOH (40 μM) was prepared in methanol (HPLC grade) and filtered using a 0.2 μm PTFE filter. A syringe pump sprayed the solution into the first vacuum chamber, using a high voltage (4 kV) needle. We also electrosprayed more concentrated solutions of TinOH but did not observe a significant increase in signal intensity. Over long time periods, solutions of TinOH in methanol are not very stable, possibly because the hydroxide anions are replaced by methoxide.[6] Therefore, we always electrosprayed fresh solutions.

9.5.2 m/z dependence of the detection efficiency

The positively charged fragments are detected on a multi-channel plate by generation of secondary electrons. The number of secondary electrons that is generated depends on the velocity of the ions. In earlier studies, the ion detection efficiency was found to be approximated by:

$$P = \frac{1 + \tanh(\frac{v-28500}{11000})}{2} \tag{9.4}$$

In Eq. 9.4, P is the detection efficiency and v is the velocity of the ion.[7] This velocity is determined by the voltage on the detector (4 kV) but also depends on the mass and charge of the ions. Using $E = \frac{1}{2}mv^2$, we obtain the ion velocity which can be substituted in the above equation. In Fig. 9.15, the dependence of the detection efficiency on m/z is shown.

Table 9.6: Selected core electron binding energies for C, O, and Sn,[8–10] main elements of the tin-oxo cage ion. Energy ranges around these binding energies were probed in the present work.

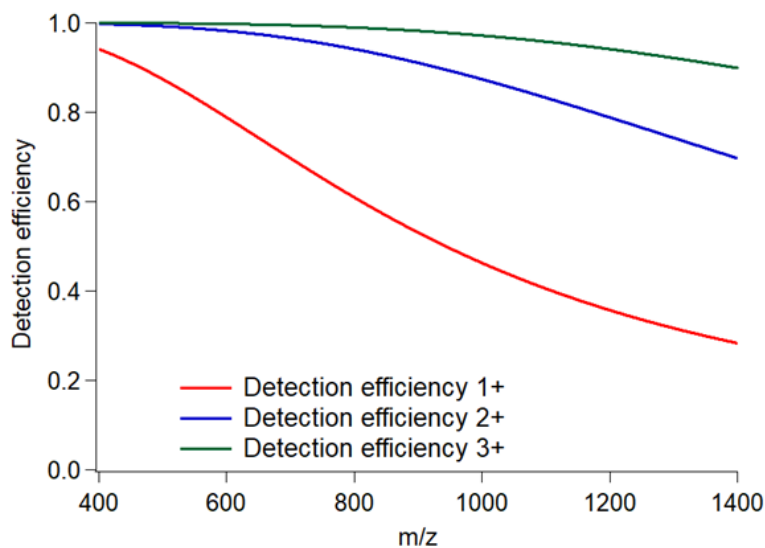| Energy/eV	Core electron orbital
23.9	Sn $4d_{5/2}$
24.9	Sn $4d_{3/2}$
83.6	Sn 4p
137.1	Sn 4s
284.2	C 1s
484.9	Sn $3d_{5/2}$
493.2	Sn $3d_{3/2}$
543.1	O 1s

16

Figure 9.15: Detection efficiency of fragments as a function of m/z. Different charges (+1 to +3) are considered. It can be seen that fragments with a higher charge are detected much more efficiently. This is corrected for in Fig. 5.4 in the main text.
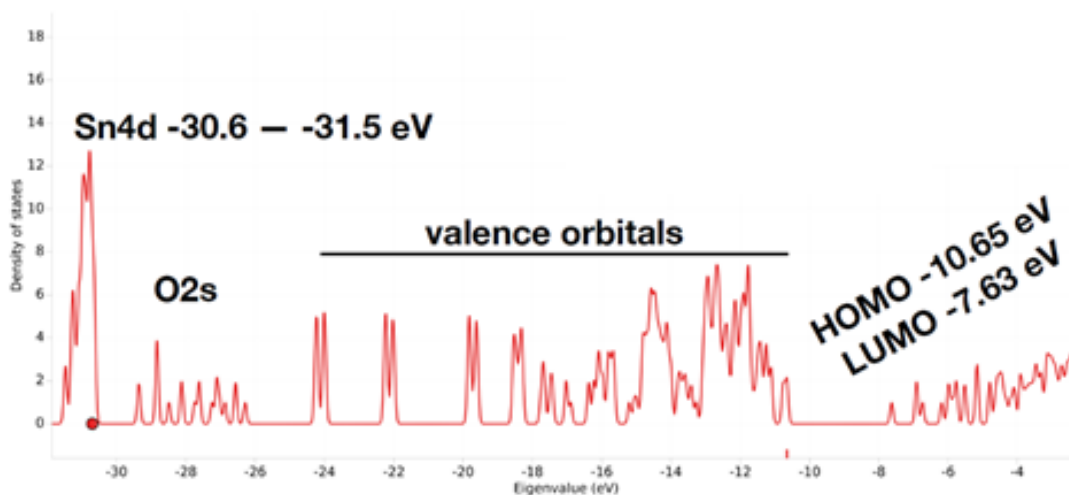

Figure 9.16: Density of states spectrum for the tin-oxo cage, with semi-core orbitals Sn 4d and O 2s (left), valence orbitals (middle) and unoccupied orbitals (right).
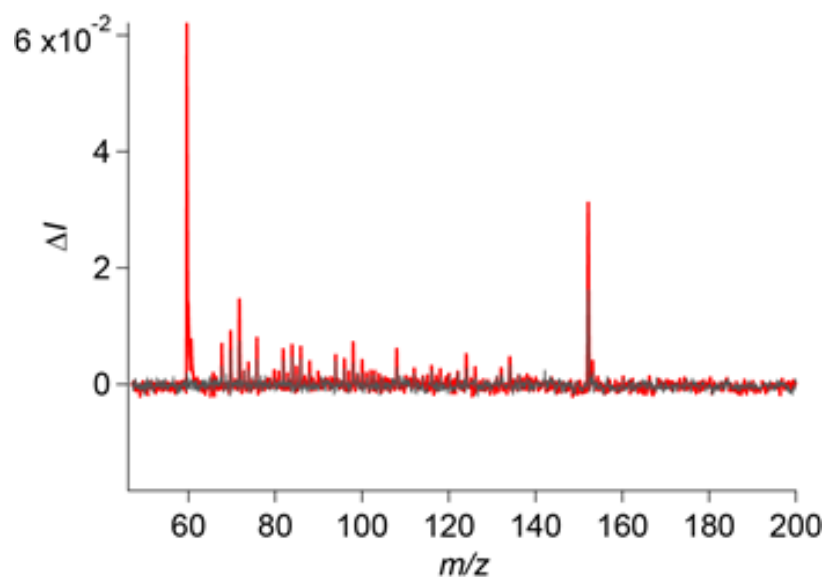
Figure 9.17: Mass spectrum in the low m/z range of the photofragmented tin-oxo cage for 91 eV photon energy (red) and background without electrospray (grey). Bu$^+$ can be seen at $m/z = 57$.
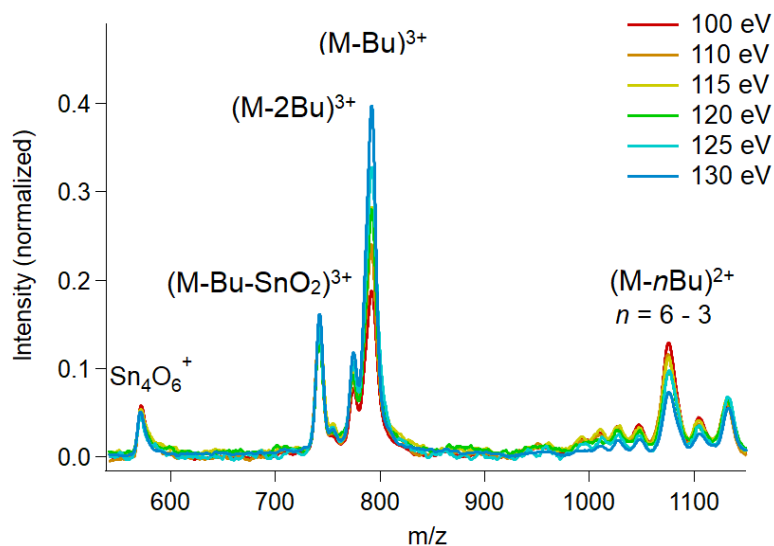

Figure 9.18: Photofragmentation spectra for photon energies 100–130 eV. A smoothing algorithm (moving average) was used for the mass spectra, to clearly distinguish the peak positions. The intensity of the peaks was normalized by setting the main peak loss to -1.
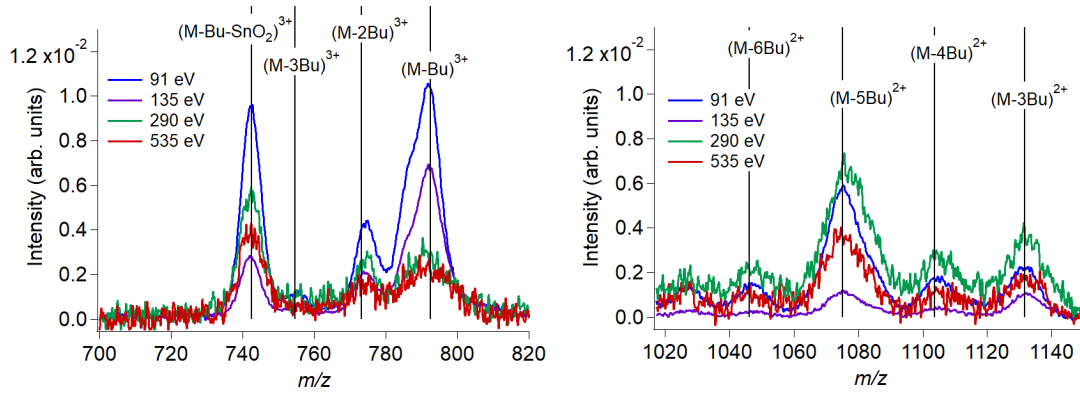
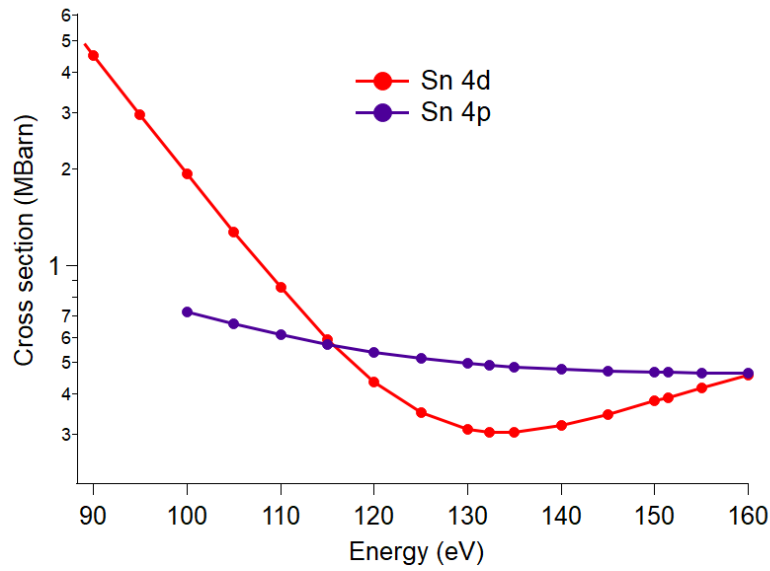Figure 9.19: Non-smoothed version of Fig. 4a (left) and Fig. 4b

Figure 9.20: Comparison between photoionization cross sections of the 4p and 4d orbitals on Sn. Tabulated values by Yeh and coworkers.[11]
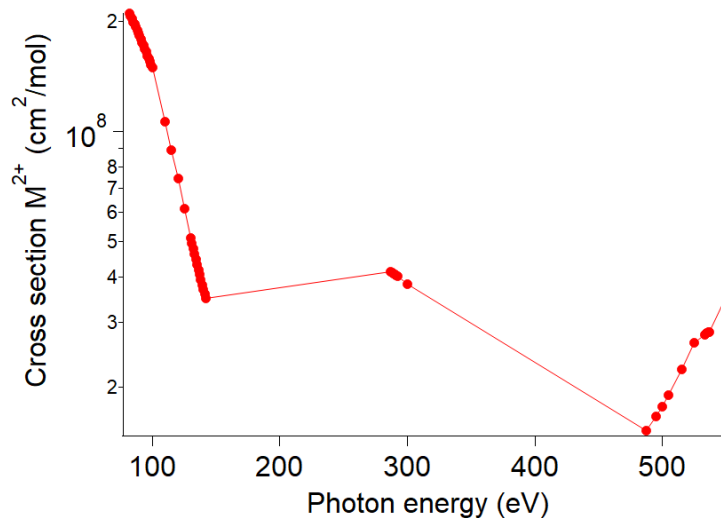
Figure 9.21: Total absorption cross section for the precursor ion M^{2+}, as a function of photon energy, for photon energies used in Chapter 5. It should be noted that these cross sections are less accurate close to absorption edges, where the cross section depends on the molecular structure.
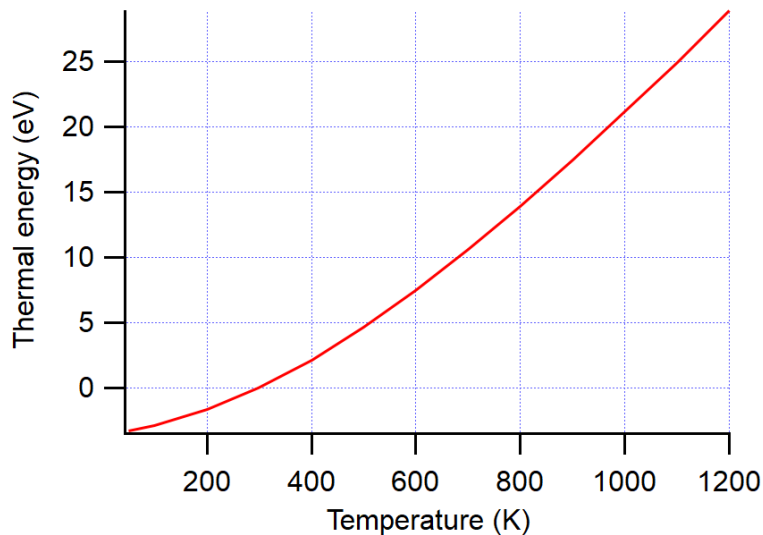

Figure 9.22: Thermal energy of the tin-oxo cage as a function of temperature, computed from vibrations of butyl tin cage. Used the DFT package B3LYP/Def2SVP, using no scaling of frequencies. Relative to $E_{\text{therm}} = 0$ at 298 K. ZPE = 1.595 eV.

9.6 Scanning transmission X-ray microscopy on tin-oxo cages
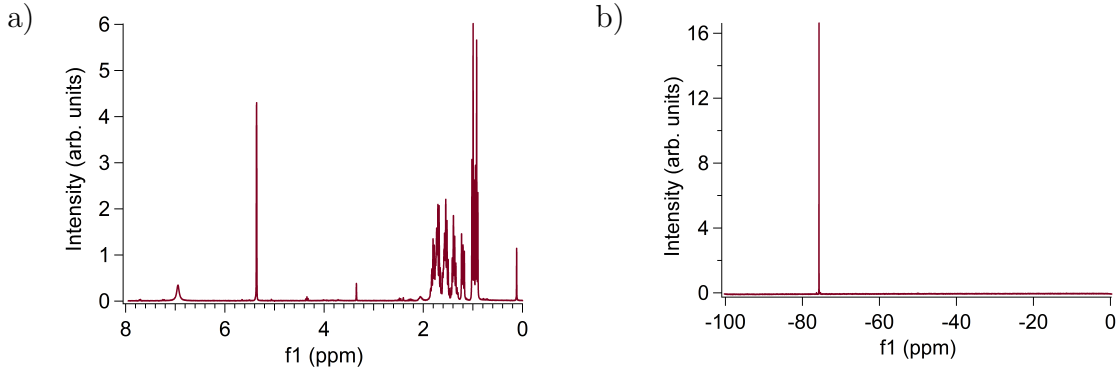
9.6.1 TinF characterization

Figure 9.23: (a) ^{1}H NMR spectrum and (b) ^{19}F NMR spectrum of TinF in CD_2Cl_2. The ^{1}H NMR shows the signals corresponding to butyl groups of the tin-oxo cage (see Chapter 3), a signal for CD_2Cl_2 (5.4 ppm) and a signal for the bridging OH groups (around 7 ppm). The ^{19}F spectrum shows that only one type of fluorine atoms is present in the material.

9.6.2 Quantum chemical calculations

9.6.3 Numerical data of atomic absorption coefficients

Table 9.7: Numerical data corresponding to Fig. 6.19 in Chapter 6. Tabulated (Tab.) values are from Ref. 10, experimental (Exp.) values are measured as described in Chapter 6.

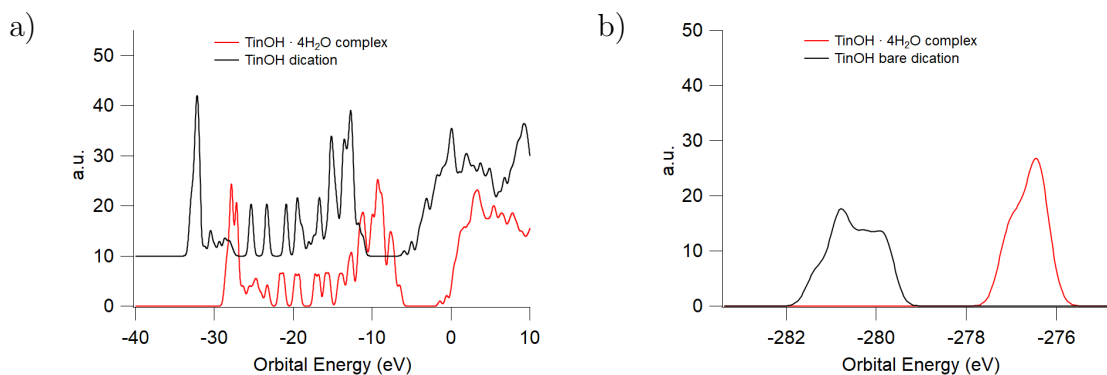| Photon energy (eV)		C σ (10^5 cm^2/mol)	O σ (10^5 cm^2/mol)	Sn σ (10^5 cm^2/mol)
320	Tab.	4.77	0.67	7.93
	Exp.	$4.97 \pm 0.2\%$	$1.09 \pm 5.3\%$	$7.60 \pm 0.7\%$
515	Tab.	1.53	0.20	12.1
	Exp.	$1.58 \pm 0.3\%$	$0.13 \pm 20\%$	$11.7 \pm 0.3\%$
550	Tab.	1.29	3.31	18.7
	Exp.	$1.32 \pm 0.7\%$	$4.12 \pm 1.4\%$	$20.1 \pm 0.4\%$

Figure 9.24: B3LYP hybrid density functional theory calculations of orbital energies: valence and semi-core (a) and carbon 1s electrons (b). The Def2TZVP basis set was used for energy evaluation and the LANL2DZP basis set was used for geometry optimization (in this case of the neutral molecule). The calculations show that the 2+ charge increases the binding energy of an(y) electron in the tin cage by 4.5–5 eV.
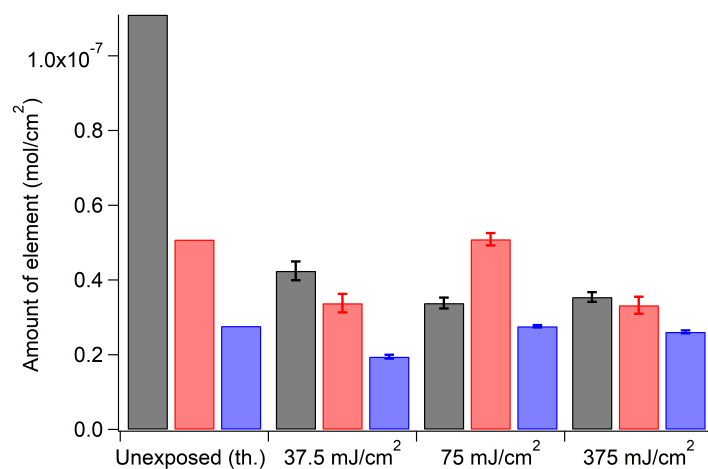
9.6.4   Duplicate of measurements on TinOH

Figure 9.25: Reproduction of measurement shown in Fig. 6.21 in Chapter 6.

Bibliography

[1] Banse, F.; Toledano, P.; Maquet, J.; Sanchez, C. Hydrolysis of monobutyltin trialkoxides: synthesis and characterizations of $\{(BuSn)_{12}O_{14}(OH)_6\}(OH)_2$. *Inorg. Chem.* **1995**, *34*, 6371–6379.

[2] Eychenne-Baron, C.; Ribot, F.; Sanchez, C. New synthesis of the nanobuilding block $\{(BuSn)_{12}O_{14}(OH)_6\}^{2+}$ and exchange properties of $\{(BuSn)_{12}O_{14}(OH)_6\}(O_3SC_6H_4CH_3)_2$. *J. Organomet. Chem.* **1998**, *567*, 137–142.

[3] Rimmelin, P.; Schwartz, S.; Sommer, J. The tetramethylammonium ion (TMA^+) versus the hydronium ion (H_3O^+) as internal reference for ^1H NMR measurements in superacid media. Solute–solvent interactions. *Org. Magn. Reson.* **1981**, *16*, 160–163.

[4] Weizman, H. Why are ^1H NMR integrations not perfect? An inquiry-based exercise for exploring the relationship between spin dynamics and NMR integration in the organic laboratory. *J. Chem. Educ.* **2008**, *85*, 294–296.

[5] Michel, D.; Böhlmann, W.; Roland, J.; Mulla-Osman, S. *Molecules in interaction with surfaces and interfaces; study of conformation and dynamics of molecules adsorbed in zeolites by ^1H NMR*; Springer, 2004; pp 217–274.

[6] Dakternieks, D.; Zhu, H.; Tiekink, E. R. T.; Colton, R. Synthesis, structure and reactions of $[(BuSn)_{12}O_{14}(OH)_6]Cl_2 \cdot 2H_2O$: solution studies using ^{119}Sn NMR and electrospray mass spectrometry. *J. Organomet. Chem.* **1994**, *476*, 33–40.

[7] Schlathölter, T.; Reitsma, G.; Egorov, D.; Gonzalez-magaça, O.; Bari, S.; Boschman, L.; Bodewits, E.; Schnorr, K.; Schmid, G.; Schröter, C. D.; Moshammer, R.; Hoekstra, R. Multiple Ionization of Free Ubiquitin Molecular Ions in Extreme Ultraviolet Free-Electron Laser Pulses. *Angew. Chem. Int. Ed.* **2016**, *55*, 1–6.

[8] Cardona, M.; Ley, L. *Photoemission in Solids I: General Principles*; Springer-Verlag, Berlin, 1978.

[9] Fuggle, J. C.; Mårtensson, N. Core-level binding energies in metals. *J. Electron Spectrosc. Relat. Phenom.* **1980**, *21*, 275–281.

[10] Henke, B. L.; Gullikson, E. M.; Davis, J. C. X-Ray interactions: photoabsorption, scattering, transmission and reflection at $E = 50$–30,000 eV, $Z = 1$–92. *At. Data Nucl. Data Tables* **1993**, *54*, 181–342.

[11] Yeh, J. J.; Lindau, I. Atomic subshell photoionization cross sections and asymmetry parameters: $1 \leq Z \leq 103$. *At. Data Nucl. Data Tables* **1985**, *32*, 1–155.